Experimental Analysis of MEMS Capacitive Accelerometer's Shock Resistibility

Yongkang Tao*, Yunfeng Liu* and Jingxin Dong*

*Department of Precision Instruments and Mechanology
Tsinghua University, Beijing, China, taoyongkang@tsinghua.org.cn

ABSTRACT

The shock resistibility of MEMS device has been an urgent issue in the field of consumer electronics, automotive industry and special military applications. The paper analyses the shock resistibility of a typical MEMS capacitive accelerometer's micro-structure by Hopkinson Pressure Bar apparatus. Experimental estimation of the three-orientation shock resistibility of the MEMS accelerometers' micro-structure has been presented, and it corresponds with the theory approximation and FEA simulations to a certain extent. Comparison of the results of different directions indicates that the spring stiffness and stoppers' areas are the key factors to determine the shock resistance. It also shows that both the pulse duration and damping ratio play critical roles in the shock effects of micro-machined structures. The paper provides meaningful guides to improve the shock reliability of MEMS accelerometers.

Keywords: shock resistibility, MEMS accelerometer, HPB, experimental estimation

1 INTRUDUCTION

Shock resistibility of MEMS (Micro-electromechanical Systems) device has become crucial in various applications. The shock amplitude during fabrication, deployment, or operation, could be as high as 5,000g-10,000g [1] with tens of μs to several ms duration time. Srikar and Stephen obtained the time-domain criteria to distinguish between the impulse, resonant and quasistatic responses of MEMS structures to shock loads [2]. Stefano investigated the effect of accidental drops on a polysilicon MEMS accelerometer within macro-scale and meso-scale finite element approach [3]. D.M. Tanner et al. performed shock experiments on a surface-micromachined micro-engine, and studied the susceptibility of MEMS devices to shock [4]. More extensive experiments on various MEMS sensors and flight tests on artillery projectiles are presented in T. G. Brown's report [5]. Multiple methods have been applied to address MEMS device reliability at every step of device design and development.

The survivability of MEMS accelerometer under high-g environment mainly includes two aspects: the integrity of micro structure and the sensor's performance change after enduring shock events. The paper analyses the shock reliability of a kind of comb-finger accelerometers' micro structure. The main objective of this study was to determine the typical failure modes and obtain an experimental estimation of MEMS accelerometers' structure due to performance change in different shock environments.

2 MEMS ACCELEROMETERS AND SHOCK EXPERIMENTS

2.1 MEMS Accelerometers

Considering a comb-finger silicon micro-machined accelerometer developed by our research group [6], the sensing element shown in Fig.1 mainly consists of movable mass, multi-fingers, spring beams and overload stoppers. The proof mass is a kind of frames with comb-fingers stretched from either side as the movable pole of the differential capacitor pair. The mass is attached to the Pyrex 7740# glass substrate by one clamped–clamped beam and four folded beams. The fixed comb fingers are anchored directly on the glass in a staggered layout with the movable comb to constitute two differential capacitors. The overload stoppers are placed both in x and y directions. Table 1 shows the typical structure parameters of the tested accelerometer.

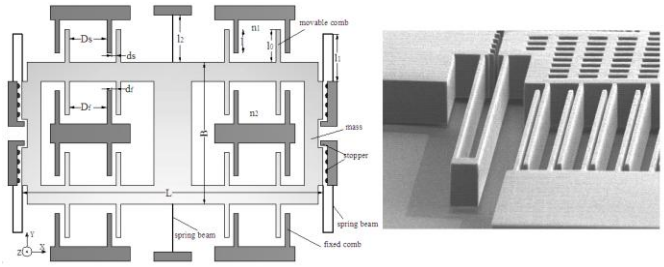

Figure 1: Simplified sketch and SEM photo of the MEMS accelerometer's structure

Items	Values	Units
sensitive mass	570	μg
stiffness of the x direction	158	N/m
stiffness of the y direction	4478	N/m
stiffness of the z direction	14430	N/m
stoppers' areas of x-axis	1800	μm^2
stoppers' areas of y-axis	600	μm^2

Table 1: Structure parameters of the accelerometer

2.2 Shock Experiments

A modified Hopkinson pressure bar (HPB) is used to load MEMS accelerometers at various shock accelerations (Figure 2). With the adjustment of gas pressure values and

energy absorb cushions made of foamed aluminum, the incident pulse could generate approximate semi sinusoidal accelerations ranging from 10^4 to 10^5 m/s^2, and the pulse width could be expanded to more than 300μs. A high-g piezoelectric accelerometer is also attached to measure the experienced shock acceleration curve. Typical shock acceleration curve is shown in Figure 3. The wave oscillation is due to stress relaxation of the crystal inside the piezoelectric sensor after high-frequency dynamic shock.

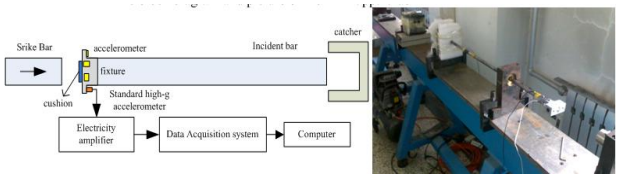

Figure 2: The block diagram and photo of the HPB

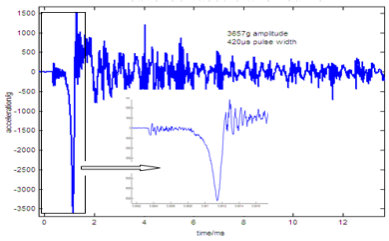

Figure 3: Typical shock acceleration curve

Shock experiments of 66 MEMS accelerometers' structures have been carried out individually in three orthogonal orientations, shown in Table 2. Micro images of the sensor structure are observed. Functionality of the accelerometers including the scale factor, zero-bias, capacitance and impedance between different poles has been measured both before and after the shock test.

Level	x-axis	y-axis	z-axis
<1,000g	2	1	3
1,000g-5,000g	9	10	9
5,000g-10,000g	7	7	3
>10,000g	7	6	2
Total samples	25	24	17

Table 2: Number of MEMS accelerometers tested at different shock level

3 THEORY APPROXIMATION AND FEA SIMULATION

3.1 Theory approximation

For the purpose of analyzing MEMS accelerometers under a shock load, some simplifying assumptions could be made as follow: (i) the package transmits the shock load to the substrate directly without damping; (ii) the acceleration is transferred to the proof mass through the spring beams; (iii) the irregular shock pulse induced is approximated by a half-sine waveform.

The accelerometer unpowered could be modeled as a second order system of mass-damp-spring. Using Laplace and inverse Laplace transform to solve the differential equation (1), the displacement response of the mass [7] to the shock pulse could be calculated as equation (2), in which k denotes the mechanical stiffness, m indicates the proof mass, and $\zeta = c/2\sqrt{mk}$ indicates the damping ratio of the system.

$$m\frac{d^2x}{dt^2} + c\frac{dx}{dt} + kx(t) = ma(t) \tag{1}$$

$$x(t) = \begin{cases} R(t) & 0 \le t \le \tau \\ R(t) + R(t-\tau) & \tau \le t \end{cases} \tag{2}$$

For different damped condition, R(t) is given by

$$\zeta < 1, R(t) = a_p \frac{\pi}{\tau}[\alpha\cos(\frac{\pi}{\tau}t) + \beta\frac{\tau}{\pi}\sin(\frac{\pi}{\tau}t) + e^{-\zeta w_n t}(\chi\cos(w_n\sqrt{1-\zeta^2}t) + \frac{\delta - \chi\zeta w_n}{w_n\sqrt{1-\zeta^2}}\sin(w_n\sqrt{1-\zeta^2}t))]$$

$$\zeta = 1, R(t) = a_p \frac{\pi}{\tau}[\alpha\cos(\frac{\pi}{\tau}t) + \beta\frac{\tau}{\pi}\sin(\frac{\pi}{\tau}t) + e^{-w_n t}(\chi + (\delta - \chi w_n)t)]$$

$$\zeta > 1, R(t) = a_p \frac{\pi}{\tau}[\alpha\cos(\frac{\pi}{\tau}t) + \beta\frac{\tau}{\pi}\sin(\frac{\pi}{\tau}t) + \eta e^{-(\zeta-\sqrt{\zeta^2-1})w_n t} + \lambda e^{-(\zeta+\sqrt{\zeta^2-1})w_n t}]$$

$$\eta = \frac{-\chi w_n(\zeta - \sqrt{\zeta^2-1}) - \delta}{2w_n\sqrt{\zeta^2-1}}, \lambda = \frac{\chi w_n(\zeta + \sqrt{\zeta^2-1}) - \delta}{2w_n\sqrt{\zeta^2-1}}$$

$$\alpha = \frac{-2\zeta w_n}{(\pi^2/\tau^2 - w_n^2)^2 + 4\zeta^2 w_n^2\pi^2/\tau^2}, \beta = \frac{w_n^2 - \pi^2/\tau^2}{(\pi^2/\tau^2 - w_n^2)^2 + 4\zeta^2 w_n^2\pi^2/\tau^2}$$

$$\chi = \frac{2\zeta w_n}{(\pi^2/\tau^2 - w_n^2)^2 + 4\zeta^2 w_n^2\pi^2/\tau^2}, \delta = \frac{4\zeta^2 w_n^2 - w_n^2 + \pi^2/\tau^2}{(\pi^2/\tau^2 - w_n^2)^2 + 4\zeta^2 w_n^2\pi^2/\tau^2}$$

As shown in above Figure 1, the flexure is composed of 5 parallel beams, and $k_x = 48EI_z/L^3$. The tested accelerometer is designed to be an under-damped system with $\zeta<1$. Theoretical approach of shock response spectrum and maximum displacement respect to duration time in different damp conditions are shown below.

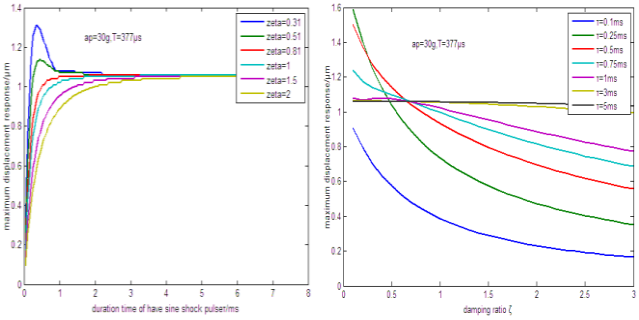

Figure 4 The shock response spectrum and maximum displacement respect to duration time of the accelerometer

The displacement response represents the maximum deformation of the spring beams, which could indicate the maximum stress distribution of the structure from a certain extent. Theory modeling shows that damping could efficiently reduce the deformation to short duration shock pulse less than 2 ms, as damping is a kind of energy consumption components. For long duration pulse, the

sensor responses quasistatically [2], and the device simply tracks the applied load. Results also indicate that pulse width plays a critical role in the dynamic shock response of MEMS accelerometers' structure. For under-damped system, there is a peak point which should be avoided by adjusting the structure's natural frequency.

For over range shock accelerations, the displacement of proof mass would exceed the minimum stopper gap. The stopper could limit the free motion while on the other hand, impact force on the contact surface of stoppers may bring other stress concentration problems. More approximate theory model should take contact into consideration.

3.2 FEA simulation

By assuming the accelerometer's structure with a certain gravity acceleration, 3D FEM simulations have been performed using ANSYS 10.0 (Figure 5). The maximum von mises stress is found at the connection place of the clamped-clamped beam due to the largest deformation. Detailed results show that the stress and deformation are proportional to the acceleration amplitude almost linearly in the static analysis. The proof mass would touch the stoppers in x direction within a 45g shock action input.

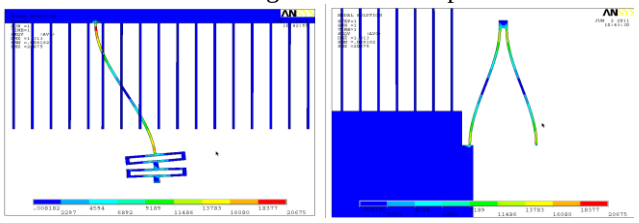

Figure 5 Static analysis by ANSYS

For shock accelerations greater than 45g, considering the effect of stoppers, dynamic FEA simulation using ANSYS/LS-DYNA is applied to calculate the structure's deformation and stress distribution under various shock amplitudes and pulse width. Both the spring beams and stoppers become fragile under the combined effects of shock inertial force and contact force. For example, ap=4000g, τ=200μs, the maximum stress appears on the stoppers at t=88μs. Figure 6 gives a comparison between the maximum stress concentration elements in clamped-clamped beam and stoppers of x direction. The stoppers endure more harsh impact than the beam (more than 100 times larger) in this example.

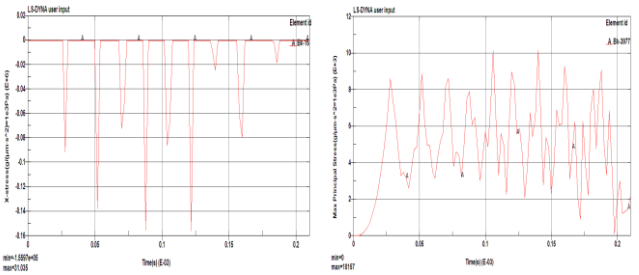

Figure 6 Time response curve of the stress distribution on stoppers and beams

4 FAILURE ANALYSIS

Failure of the micro structure after HPB shock experiments has been observed in different parts of the accelerometers, such as spring beams, stoppers, proof mass peripheral frames and so on, while the comb-fingers, bonding pads and die package shell are rather robust to shock. Several micro images of failure modes are shown in Figure 7. Failure types on the spring beams appear as deformation, cracks, partial pitting, fracture of several beams and complete fracture of total beams. Failures of the stoppers are shown as cracks, pitting, collapse, partially damaged and totally damaged. Failures of the peripheral frames are classified into pitting, cracks and fractures. Pitting of the proof mass on the contact area with the stoppers could also be observed.

Typically more than 2 failure types could appear under one shot, and some failure types are specific to a particular shock direction and amplitude range, while some of them always occur in company with each other. A full discussion of the results and failure analysis in three orientations respect to various amplitudes and pulse width are shown below.

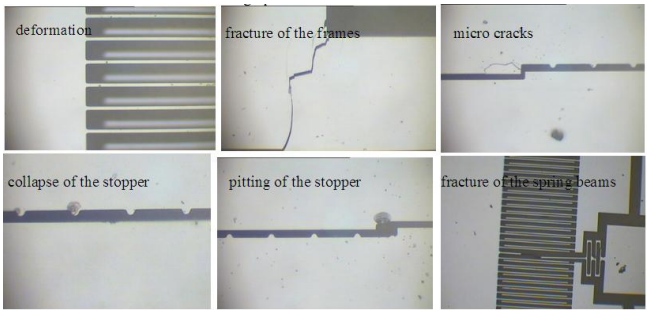

Figure 7 Micro images of different failure modes

4.1 x-direction results

All tested accelerometers have exhibited no damage at shock levels less than 1,000g in x direction. Micro cracks and fractures of the peripheral frames appeared under 1469g, 360μs; 2964g, 390μs and 4489g, 360μs shock levels. At 2106g, 330μs shock action, cracks have been found on the buffer structure of the clamped-clamped beam which doesn't affect the practical function of the beams. Long duration shock pulse could lead to deformation of the spring beams, observed at the load of 2330g, 875μs.

Severe failure types have occurred in the 14 tested specimens at shock levels more than 6000g, such as fractures of 3-4 spring beams (7145g, 300μs; 7244g, 335μs; 7754g, 269μs) and large deformation of the beams (6179g, 300μs) in z direction. As the proof mass would twist under continued shock impact after it has touched the x-direction stoppers, both the stoppers in x and y direction have been found damaged. Fractures of partial beams reduce the support force of the proof mass, which could result in large deformation in z-direction.

4.2 y-direction results

No failures happened at shock levels less than 5,000g in y-direction. Failures only occurred at the y-direction stoppers including micro cracks, pitting and collapse, when the shock amplitude is ranged from 5,000g to 7,000g. Two folded beams fractured on the tested micro structure at 7244g, 335μs shock.

Experiment results show that the tested accelerometer could resist larger shock impact in y direction. It's mainly determined by the mechanical stiffness. The stiffer the beams are, the less deformation would occur under high-g shock.

4.3 z-direction results

The micro structure is weakest in z-direction as it has no stopper to limit the motion. Spring beams begin to fracture at the shock level of 3000g, and shock amplitudes more than 4,000g would lead to complete fractures of total beams. In fact, k_z is much bigger than k_x as shown in Table 1, but overload stoppers are designed in x-direction. Comparison of the experimental results between x and z direction indicates that the stopper is a critical factor in the shock reliability of MEMS sensors. Stoppers could limit the deformation of the micro structure and transmit the induced shock energy partially, which could reduce and share responsibility for the stress concentration. in the micro structures.

5 EXPERIMENTAL ESTIMATION OF SHOCK RESISTIBILITY

Sensors are supposed to function normally with little performance change after enduring shock events. On the basis of the influence on the open-loop performance of the accelerometer, failure types could be classified into three levels: 1. Almost normal, the accelerometer could practically work as usual; 2. Partially available, the performance has changed but the device could still operate; 3. Totally damaged, the device could not be used any more. Level 1 consists of failures of the stoppers and frames. Level 2 includes the small deformation and fractures of several spring beams, which would affect the accelerometer's scale factor and zero bias. Level 3 happens as the proof mass falls off from the glass substrate due to the complete fractures of total beams.

According to the above classification, experiment estimation of the three-orientation shock resistibility of the MEMS accelerometers' micro-structure, is shown in Figure 8 in detail. The area surrounded by the green line, the longitudinal and horizontal axis gives a safe range of shock amplitudes and pulse width. Long duration pulse would allow low shock amplitudes as the fracture stress criteria is concerned with the induced energy to a certain extent. The image at the bottom right corner gives an experimental evaluation of the shock reliability in three directions.

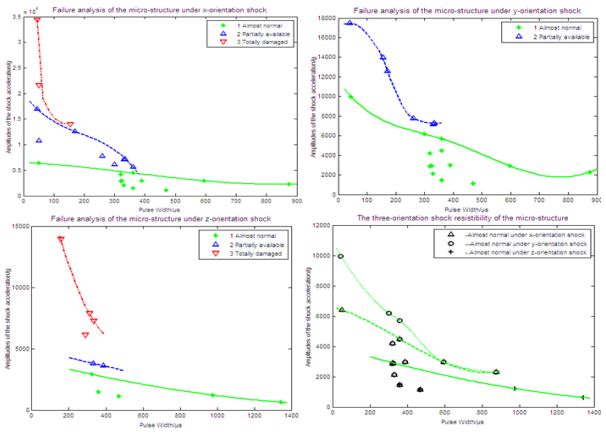

Figure 8 Experiment estimation of the three-orientation shock resistibility

6 CONCLUSION

Analysis of the tested accelerometers indicates that the spring stiffness and stoppers' areas are the key factors to determine the shock resistance. Research also shows that both the pulse duration and damping ratio play critical roles in the shock effects of micro-machined structures. The paper provides meaningful guides to improve the shock reliability of MEMS accelerometers. The research methods mentioned may also be applied to the estimation of the shock reliability of other MEMS device.

REFERENCE

[1] Rob O'Reilly, Huy Tang,Wei Chen. High-g Testing of MEMS Devices, and Why [C]//. Proceedings of IEEE Sensors, 2008:148-151.

[2] V. T. Srikar , Stephen D. Senturia. The reliability of microelectromechanical systems (MEMS) in shock environments[J].Journal of Microelectromechanical systems, 2002, 11(3): 206-213.

[3] Stefano Mariani,Aldo Ghisi,et al. Multi-scale Analysis of MEMS Sensors Subject to Drop Impacts[J]. Sensors 2007,1817-1833

[4] Tanner, D.M., Walraven, J.A, et al. MEMS Reliability in Shock Environments [C]//. Reliability Physics Symposium, 2000. Proceedings. 38th Annual 2000 IEEE International:129-138.

[5] T. G. Brown and B. Davis, Dynamic High-G Loading of MEMS Sensors: Ground and Flight Testing, SPlE Proceeding, Vol 3512, 1998, pp. 228-235.

[6] Dong Jingxin, et al. Micro inertial instruments-micromachined accelerometer[M]. Beijing: Tsinghua University, 2002.

[7] Subramanian Sundaram, Maurizio Tormen, et.al. Vibration and shock reliability of MEMS:modeling and experimental validation[J]. Journal of Micromechanical and microengineering: 2011,21:1-13.